THE JOURNAL OF PHYSICAL CHEMISTRY C

Article

Formation and Atomic Structure of Hierarchical Boron Nitride Nanostructures

Ramon Antonio Silva-Molina, Emilio Muñoz-Sandoval,
Rogelio Gámez Corrales, and Ricardo A. Guirado-Lopez

J. Phys. Chem. C, **Just Accepted Manuscript** • DOI: 10.1021/acs.jpcc.5b07061 • Publication Date (Web): 23 Oct 2015

Formation and Atomic Structure of Hierarchical Boron Nitride Nanostructures

R.A. Silva-Molina[1], E. Muñoz-Sandoval[2], R. Gámez-Corrales[3], and R. A. Guirado-López[1],*

[1] *Instituto de Física "Manuel Sandoval Vallarta", Universidad Autónoma de San Luis Potosí, Álvaro Obregón 64, 78000, San Luis Potosí, SLP, México*

[2] *Advanced Materials Department, IPICyT, Camino a la Presa San José 2055, Col. Lomas 4a. sección, San Luis Potosí 78216, SLP, México*

[3] *Departamento de Física, Universidad de Sonora, Apartado Postal 5-088, 83190, Hermosillo, Sonora, México4441193877*

Abstract

In this work we report a combined experimental and theoretical study of boron nitride (BN) nanostructures synthesized by ball milling methodology. The BN nanostructures were obtained using *h*-BN powder under low vacuum conditions and steel balls of different sizes. The HRTEM images of our samples show the formation of spheroidal BN nanoparticles with diameters as small as ~7 nm which self-assemble into different hierarchical nanostructures such as two-dimensional layered materials, spheroidal configurations, and one-dimensional solid BN chains. The Raman spectra reveals an intense absorption band in the 300—600 cm^{-1} region, which is absent in the spectra of BN nanotubes, previously synthesized BN nanoparticles, as well as in all bulk boron-nitride polymorphs. Density functional theory calculations show that the Raman spectra is consistent with the formation of fullerene-like BN particles which also exhibit an intense absorption band in the 200—800 cm^{-1} range dominated by a complex mixture of tangential, stretching, and radial breathing modes. Finally, by means of electron-beam irradiation experiments additional structural transformations can be induce on our hierarchical BN particles consisting in the

* Corresponding author. E-mail: guirado@ifisica.uaslp.mx (Ricardo A. Guirado-López)

formation of nano-holes of the order of 5 nm. Our here-reported BN nanostructures might lead to a wide range of potential applications.

Keywords: boron nitride, ball milling, density functional theory

Introduction

One of the most studied bulk layered materials in the last years is boron nitride in its hexagonal form due to its properties suitable for a wide range of applications[1-4]. The hexagonal *h*-BN structure is the most stable among BN polymorphs (when compared to the cubic and wurtzite BN) and, within each layer, boron and nitrogen atoms are strongly bonded whereas the layers are held together by weak van der Waals forces similar to graphite. Consequently, *h*-BN is employed as a lubricant (at both low and high temperatures)[5] as well as protective and optical coatings[6]. Boron nitride ceramics are also typically used as parts of high-temperature equipment[7] and, in the electronics industry, as substrates for semiconductors as well as a structural material for seals[8].

Other forms of boron nitride have been reported in the literature motivated by the increasing efforts intended to achieve the nanostructuration of BN. Boron nitride nanotubes were predicted in 1994[9] and experimentally synthesized in 1995[10]. The properties of BN nanotubes were found to be different from those obtained for carbon nanotubes. While the laters can be metallic or semiconducting depending on the rolling direction and radius, the formers are defined by an insulating behavior with a wide bandgap of ~5.5 eV, being independent of tube diameter, helicity, length, and number of walls[11]. Boron-nitride nanotubes are characterized by a high thermal and chemical stability which defines them also as promising materials to be used in in hazardous and high temperature environments[12].

Spheroidal BN nanoparticles have also attracted the interest of the scientific community since they exhibit a higher surface area than nanomaterials with other morphologies. In addition, the production of BN particles with reduced diameters will allow its effective

inclusion in different types of matrices forming various kinds of composite materials. The elaboration of BN nanoparticles has been undertaken by two main approaches: bottom-up and top-down methodologies. The former procedure involves the synthesis of BN nanostructures from boron- and nitrogen-containing molecular precursors using the chemical vapor deposition (CVD) method [13]. In the later, mechanical cleavage, sonication-assisted exfoliation, and BN nanotube unzipping are the most employed approaches. With the use of the previous methodologies a large variety of BN nanoparticles with different sizes and morphologies have been produced and interesting trends have been revealed. For example, Tang et al.[14] synthesized spherical boron nitride nanoparticles by the chemical vapor deposition reaction of trimethoxyborane [$B(OMe)_3$] with ammonia, followed by high temperature annealing. The as-synthesized BN spheres had diameters varying from 50 to 400 nm and contained O and C impurities. The presence of oxygen impurities was found to play a fundamental role in defining the size and the spherical morphology of BN nanostructures. High oxygen-containing BN spheres (~6.3 wt %) had diameters of ~90 nm while low oxygen-containing BN structures (<1 wt %) were characterized by particle diameters of ~30 nm. Interestingly, the spherical morphology is fully collapsed after annealing the samples at 1800 °C when all oxygen species are removed under a high-temperature ammonothermal reaction.

Salles and co-workers[15] prepared ultrafine boron nitride powders by the spray-pyrolysis of borazine. The as-synthesized samples were formed by elementary blocks containing slightly agglomerated and round-shape BN nanoparticles with sizes ranging from 55 to 120 nm and a Brunauer-Emmett-Teller (BET)-specific surface area of 34.6 $m^2 g^{-1}$. They showed that these ultrafine powders could be employed to fabricate microstructured disk-shaped

boron-nitride materials with a high relative density (96.3%) and a homogeneous microstructure. Actually, they can be also used as precursors to produce large quantities of hollow boron nitride nanopolyhedrons[16]. These novel architectures are interesting since they have been generated via a solid-state transformation in relatively high yields and without a metal catalyst. The average size of these nanostructures vary from 20 to 40 nm in diameter, they are highly crystalline and characterized by having 15-20 concentric layers with an interlayer distance of 3.3 Å. We emphasize the work of Koi et al.[17] where the fabrication of huge boron nitride nanocages (with sizes ranging from 200 nm to 1 μm) was reported by annealing Fe_4N and B powders at 1000 °C for 1 h in nitrogen gas atmosphere. These BN cages exhibit photo-luminescence spectra characterized by a broad peak centered at 3.8 eV (327 nm). This cage structures with both electrical and atmospheric insulation are expected to be very useful as efficient nano-containers in gas storage applications.

Finally, we mention that BN structures in the small cluster regime have been also synthesized by Goldberg and co-workers [18]. They reported the formation of boron-nitride fullerenes with a reduced number of layers (up to three) in hexagonal BN flakes which were subjected to in situ electron irradiation at 20 and 490 °C in a high resolution 300 keV transmission electron microscope. The as-synthesized BN fullerenes exhibited B/N stoichiometry of ~1 and corroborated the octahedral BN fullerene growth model proposed in Ref.[19] where square-like BN rings are the key structural blocks in these spheroidal arrays. Similar fullerene-like BN clusters were synthesized by Oku et al. [20] employing the arc-melting method in nitrogen gas atmosphere.

At this point it is important to comment that the potential use of the BN nanostructures mentioned above for physical hydrogen storage is high [21-22], as well as its use as catalyst

support or gas adsorbent. In addition, the surface of BN nanostructures is expected to be hydrophobic in nature, a fact that can prevent moisture condensation. However, realizing the previous applications requires the implementation of synthesis protocols which can allow its large scale production, that preferably do not use of organic solvents as precursors, and that could lead to homogeneous distributions of small and round shape BN nanoparticles. Furthermore, the possibility of fabricating additional nanostructures with these nanoparticles forming more complex BN materials could lead to novel applications.

In this work, we report the synthesis of spheroidal BN nanoparticles by using low-cost an efficient ball milling mixing process as the main fabrication step. We show that by varying the milling hours and annealing time it is possible to play with the nanostructuration of the starting *h*-BN material. Complete characterization of the samples by Scanning Electron Microscopy (SEM), High Resolution Transmission Electron Microscopy (HRTEM) and X-Ray Diffraction (XRD) demonstrate that we have obtained boron-nitride nanoparticles with diameters as small as 7 nm, which self-assemble to form hierarchical two-dimensional layered structures, spheroidal configurations, and one-dimensional chain-like morphologies. The Raman spectrum of our BN nanostructures is characterized by an intense absorption band in the 300—600 cm^{-1} region. According to our density functional theory (DFT) calculations the measured spectra seems to be consistent with the formation of onion-like fullerene BN particles characterized also by an intense absorption band in the 200—600 cm^{-1} range. The X-Ray Photoelectron Spectroscopy (XPS) data reveals the presence of oxygen impurities in the surface of the particles which could be responsible for the expanded interlayer distance as well as for the unusually large B—N bond lengths inferred from HRTEM images. Finally, we suggest that electron-beam irradiation

experiments could be used to perform controlled modifications of the structure of our BN materials and additionally tune the morphology of our samples.

2. Experimental Section

2.1 Ball Milling. Commercially available *h*-BN powder with 99.5% purity was used as starting material. An amount of 0.5 g of this material was ball milled during 100 h at room temperature using planetary ball mill FRITSCH equipment. A total of 56 pieces of steel balls of six different sizes, and with diameters varying from 3 to 8 mm, were introduced in the stainless steel vials together with the *h*-BN powder. The ball milling process was performed under low vacuum conditions (1.01 bars) obtained by a mechanical pump. The resulting fine powder was further annealed under 1.01 bars of vacuum at 1000 °C during 16 h. No inert gas within the chamber was employed.

2.2. Structural Characterization. The general morphology of both milled and annealed samples at different times was characterized by SEM using a FEI Helios 600 Nanolab dual beam system. Energy Dispersive X-Ray spectroscopy (EDX) spectra were recorded during SEM observations for determining the stoichiometry and chemical states of the samples. To refine the structural information we employ 300 KeV HRTEM FEI TECNAI F30 STWIN G2 equipment. In addition, we will perform electron beam irradiation experiments on our synthesized BN nanostructures. Focused electron beams on boron nitride materials for short periods of time can induce damage and disordering, considerably affecting the properties of the samples. Despite the practical importance of this kind of experiments, we believe that the influence of electron beam irradiation on BN nanostructures has not been extensively reported and is clearly of fundamental science interest. Finally, the crystalline structure of

our BN samples was also investigated at room temperature by XRD analysis using a Bruker AXS equipment with Cu Kα (λ=0.15405 nm) radiation.

2.3. FTIR, Raman Spectroscopy, and Chemical Composition. The FTIR were carried out using Perkin Elmer FTIR 1600 with KBr pellet from 450 to 4000 $cm^{-1}$and the Raman spectra of our samples were obtained using Horiba Jobin Yvon micro-Raman equipment employing a laser wavelength of 532 nm (20 mW power). A 2400 g/mm spectral field was used with a dispersion of 6.5 cm^{-1}/mm and a 2 cm^{-1} to 15 cm^{-1} resolution. The chemical composition was determined through XPS measurements employing Perkin Elmer PHI5100 equipment with a 0.025 eV resolution. In addition to compositional analysis, XPS has provided us with information related with the chemical environment of B and N species based on the peak-fitting of XP spectral envelopes.

3. Theoretical Calculations. The structural, electronic, and vibrational properties of model boron nitride particles have been obtained within the DFT approach with the help of the GAUSSIAN09[23] software. The Kohn-Sham equations were solved employing the Perdew-Burke-Ernzerhof (PBE)[24] expression for the exchange-correlation potential together with the 3-21g basis set[25] which is a good compromise between computational costs and accuracy. In all cases, fully unconstrained spin-polarized structural optimizations for all our considered isomers were performed using the conjugate gradient method. The vibrational frequencies have been determined by diagonalization of the full Hessian matrix within the harmonic approximation. This procedure generates all vibrational modes of the molecular structures which can be directly compared with experimental infrared and Raman spectroscopy measurements. We must precise that, due to the large differences in the

electronegativities of the elements involved we expect the existence of a very inhomogeneous electron density distribution in our BN particles having both highly positively and negatively charged atoms. This non-uniform distribution of charge is expected to lead to a complex distribution of attractive and repulsive electrostatic interactions that will be of fundamental importance in determining the stability of our systems.

4. Results and Discussion

4.1 Formation of Hierarchical BN Nanostructures. The morphologies of the samples were investigated by performing an extensive SEM characterization. In Fig. 1 we show first the SEM images of our samples at ambient temperature for different milling times. At 10 h of milling [Figs. 1(a) and 1(b)] we observe the spontaneous formation of elementary blocks of irregular shape composed of agglomerated BN nanoparticles. Interestingly, at 50 h [Fig. 1(c)], the dimensionality of the self-organization changes and it is now possible to observe BN spheres forming two-dimensional islands [as shown more clearly in Fig. 1(d) which corresponds to a high magnification image of the selected area shown in Fig. 1(c)]. Finally, after 100 h of milling [Figs. 1(e)] the agglomeration of boron-nitride nanoparticles increases leading to the existence of extended layers with high surface area, well-defined edges, and rough surfaces [see Fig. 1(f) for the selected area of the sample shown in Fig. 1(e)]. The previous spontaneous formation of hierarchical nanostructures where BN nanoparticles jointly participate in their construction is intriguing and clearly illustrates how, by monitoring the milling hours, it is possible to control the nano-structuration of the starting *h*-BN material.

Further annealing of the samples after 100 h of milling reveals also interesting trends. In Fig. 2 we present SEM images after heating the samples at 1000 °C during 16 h that show additional transformations of our nanostructured material. From Fig. 2(a) and 2(b) we remark that, besides the existence of extended planes made of small BN nanoparticle subunits, it is possible to distinguish the formation of hierarchical spheroidal structures which spontaneously nucleate from well-defined sites on the BN layers and grow at expense of the neighboring local atomic environment [see Fig. 2(b)] (i.e., fusion of the small BN particles to produce larger hierarchical boron-nitride spheres). By taking a closer look to our samples we see from Figs. 2(c) and 2(d), as representative examples, the existence of BN hierarchical spheres with diameters of the order of 1 μm and 400 nm, respectively, having rough surfaces, and being formed by a large number of densely packed small BN particles. Finally, we note from Figs. 2(e) and 2(f) that a one-dimensional type of nanoparticle aggregation is also possible leading to the formation of solid BN chains. As is well known, this type of one-dimensional organization is relevant and will be needed for nano-wiring processes in future electronic devices. In all cases the SEM images reveals a notable poly-dispersity for the spherical particles, a fact that must be of fundamental importance for the stability and aggregation behavior of these complex systems. It is thus clear that our here-obtained nanoparticle systems are metastable and that further temperature variations could lead to notable (additional) structural transformations that might produce novel nanostructures with useful material properties.

4.2 X-ray Diffraction (XRD). Shown in Fig. 3 are the X-ray diffraction patterns of our BN nanostructures at different milling times. XRD was carried out at room temperature using Cu Kα radiation (λ=0.154 nm). When compared with the pattern of starting *h*-BN (black

line) we appreciate that formation of BN nanomaterials shown in Fig. 1 considerably broaden the XRD data. From the figure we see the existence of two very broad diffraction peaks at 2θ=24.8 and 44.5 degrees. In particular the (002) peak slightly shifts to lower angles when compared to the bulk data (a well-known displacement observed in the XRD pattern of similar nanostructured BN materials) a behavior that has been correlated with the poor crystallization (layer disorder) of our synthesized material (formation of a turbostratic structure), expansions in the interlayer distances due to local curvature effects, and to the presence of impurities within the layers. Interestingly, and despite the complex structural evolution shown in Fig. 1, we can appreciate that the XRD patterns for different milling hours remain essentially the same.

4.3 HRTEM Characterization. Fig. 4 shows typical HRTEM images of our BN samples after 100 h of milling. As evidenced by SEM we appreciate from Figs. 4(a) and 4(b) [which corresponds to a high magnification image of the selected area shown in Fig. 4(a)] several spheroidal BN units of different sizes which are aggregated to form a larger particle with an irregular shape and an average diameter of ~200 nm [Fig. 4(a)]. Additionally, we observe from Fig. 4(a) that the packing of the BN particles is not high and that there is empty space inside the BN nanostructures, a result that could be of fundamental importance for gas storage and catalytic applications of these materials. Interestingly, Figs. 4(c) and 4(d) show HRTEM images of two isolated BN nanoparticles. From these figures we can determine particle diameters of ~7 nm which are among the smallest values found in the literature for these kinds of systems. These and other similar images exhibit sharp lattice fringes (marked by arrows) which define interlayer distances varying from 3.3—3.8 Å, the formers corresponding to expanded BN planes due to the existence of curved layers and the

presence of impurities within the boron-nitride nanoparticles[26-14]. Interestingly, we have also obtained a set of reduced interatomic distances ranging from 1.4 to 2.3 Å which, as we will see in the following, seem to correspond to the presence of oxygen impurities in the surface of our as-synthesized boron-nitride nanostructures.

Besides providing precise details of the local atomic structure, electron-beam irradiation has been found to be also a powerful tool for the synthesis, controlled modification, and characterization of nanostructured materials. In particular, creating nano-holes on semiconducting or metallic nanoparticles could lead to interesting electronic, optical, and catalytic properties. Taking advantage of the huge size of some of our synthesized BN spheres we have performed electron beam irradiation experiments on pre-existing boron nitride hierarchical nanostructures, as the ones shown in Figs. 2(c) and 2(d). In Fig. 5, we show the HRTEM image of an isolated hierarchical BN sphere of ~300 nm in diameter which was subjected to an incident electron beam of 300 keV for 2 min. The intense electron irradiation resulted in the removal of a large amount of atoms from the surface leading to the formation of a notable hole (marked with an arrow) of approximately 50 nm in diameter which can allow the inclusion of a large variety of atomic and molecular species. It is important to remark that electron beam irradiation in these samples does not result in destructive effects but can be used in a creative way to improve the functionality of our materials.

4.4 XPS Analysis. The chemical composition of our as-synthesized BN nanostructures can be derived from the XPS spectra shown in Fig. 6. The XPS data shown in the figure correspond to typical survey spectra from different milling hours and clearly indicate the presence of B and N elements, as well as the existence of carbon and oxygen impurities.

These impurity peaks could have been originated by the adsorption of CO_2 and O_2 onto the surface of our samples due to the low vacuum conditions employed in our synthesis. However, and as clearly stated by Tang et al.[14], the stability of spheroidal BN nanoparticles is strongly correlated with the amount of impurity oxygen present in the BN material. Oxygen can be removed at temperatures of the order of 1800 °C; however, the previous thermal conditions are well above the ones used in our synthesis procedure. Finally, we have found that the B/N ratio is ~0.9 which highlights the stable and inert B—N bonding.

The key spectral regions shown in Fig. 6 are boron B 1s and nitrogen N 1s. Both B 1s and N 1s peaks are shown in detail in Figs. 7(a) and 7(b), respectively, for a BN sample after 100 h of milling (blue line in Fig. 6). We remark first that the asymmetric shapes of boron and nitrogen spectra (see the red lines) reveal that several types of boron and nitrogen bonds are present in the structures. Notice that the binding energies centered at 190.5 eV for B 1s and 398.3 eV for N 1s are in good agreement with the values found for bulk *h*-BN. However, in the particular case of N 1s [Fig. 7(b)] we observe that the slight asymmetries in both high and low energy sides requires the inclusion of additional contributions centered at binding energies of 401.1, 399.7, and 396.2 eV which defines the presence of N—O, N—O—B, and N—Fe type of bonds, respectively. The small amount of detected iron could be attributed to a low level contamination from the reaction vessel and/or from the steel balls during the milling process. Similar trends are observed in Fig. 7(a) where the best fit (red line) to the B 1s peak is achieved by including three additional gaussians centered at 193.1, 191.7, and 188.4 eV which are binding energies that imply the existence of B—O, B—O—N, and B—C bonds, respectively. Notice that the fit of the B 1s envelope does not require the presence of B—Fe bonds (a contribution located in the 187.8—188 eV energy range) however boron sites seem to be oxidized.

4.4 Infrared and Raman Spectroscopy. As is well known, vibrational spectroscopy (both Raman and infrared) is an additional powerful technique to characterize the structure and chemical composition of our as-synthesized materials. The infrared and Raman spectra of our BN nanostructures at 10, 50, and 100 h of milling are shown in Figs. 8 and 9, respectively, and reveal interesting features. The infrared spectra reveals in all cases the existence of a very intense absorption band located at 1350 cm^{-1} followed by a broad and small peak placed around 1000 cm^{-1}. Below 800 cm^{-1} we observe and additional double peak contribution of low intensity whose structure and location is almost independent of the milling hours. Similar infrared spectra have been obtained by Tang et al. and co-workers in ultra-fine powders made of spherical BN nanoparticles. In the case of the Raman characterization, the spectra shown in Fig. 9 are marked by the presence of a double peak structure located in the 300—600 cm^{-1} region, whose intensity is comparable in all three cases. Notice also the complete absence of the *h*-BN adsorption band (see the black line) typically located at 1360 cm^{-1} which corresponds to the B—N in-plane atomic displacements. These spectral features are completely absent in the Raman characterization of i) *h*-BN and all bulk boron-nitride polymorphs [27], ii) BN nanotubes (both single and multi-walled)[28], as well as iii) in previously synthesized BN nanoparticles. Clearly, the observed features in the infrared and Raman spectra of our samples can be assigned to definite vibrational modes if the corresponding intensities can be predicted as well. Consequently, in the next section, we present extensive DFT calculations on model BN nanoparticles in order to achieve a possible identification of the structure by infrared and Raman spectroscopies.

DFT studies. Following the experimental Raman spectra shown in Fig. 9 and its corresponding comparison with available data of various BN nanostructured materials we propose that our synthesized BN particles could be defined by onion-like fullerene configurations. BN particles having fullerene-like structures have been already synthesized by Oku et al. [29] using the arc-melting method of an YB_6 powder in a N_2/Ar mixture gas and later on detected by time of flight mass spectrometry. They have been found also in electron-beam irradiation experiments performed by Golberg et al. [18] on hexagonal BN flakes. In this case, HRTEM images reveal the presence of BN fullerenes with small diameters varying from 1.1—1.4 nm and having the stoichiometry of B/N~1. Various spheroidal structural models have been proposed for these BN fullerenes the smallest one being the $B_{12}N_{12}$ [30] cage and among the largest ones the $B_{48}N_{48}$ [31] structure, all of them consisting of only 4- and 6-membered BN rings. Here, we combine these two atomic configurations in order to construct an onion-like array of the form $B_{12}N_{12}@B_{48}N_{48}$ (yielding a 120-atom structure) and analyze its stability, electronic properties, and vibrational behavior. Clearly, our here-proposed structural model is far from the actual experimental situation however, we believe it contains the fundamental physical interactions and precise details of the local atomic environment of these kinds of systems. In Fig. 10 we show the lowest energy configuration (as insets) and the simulated infrared spectra of $B_{12}N_{12}$ [Fig. 10(a)], $B_{48}N_{48}$ [Fig. 10(b)], and $B_{12}N_{12}@B_{48}N_{48}$ [Fig. 10(c)] fullerenes. The infrared intensities have been broadened by 25 cm^{-1} to mimic experimental uncertainties. From Figs. 10(a) and 10(b) we notice the existence of highly stable BN structures having only positive vibrational frequencies implying the high stability of the model structures. Notice from Fig. 10(c) that our here-proposed onion-like $B_{12}N_{12}@B_{48}N_{48}$ configuration is also stable and its vibrational spectra is a superposition of both Figs. 10(a)

and 10(b). Finally, we found that in Fig. 10(c) the most intense bands located around 1400 and 780 cm^{-1} are defined by complex tangential as well as radial breathing modes, respectively, and that we have a very nice agreement between our simulated spectra and the measured data shown in Fig. 8.

In Fig. 11 we present the average density of states (DOS) of our model BN particles. From Figs. 11(a) and 11(b) we note the existence of large HOMO—LUMO energy gaps of the order of 4.2 eV, as already reported in the literature [32]. In addition, the calculation of Mulliken charges reveal that our model BN clusters are molecules with polarity because of a positive charge at boron atom positions and a negative charge at N positions enable them to disperse in polar solvents. Finally, from Fig. 11(c) we find a reduced (but still large) HOMO—LUMO gap of 3 eV so we predict that our onion-like fullerene configuration will not be able to absorb energies in the visible region of the spectra.

In Fig. 12 we plot now our calculated Raman spectra for our model $B_{12}N_{12}$ [Fig. 12(a)], $B_{48}N_{48}$ [Fig. 12(b)], and $B_{12}N_{12}@B_{48}N_{48}$ [Fig. 12(c)] fullerenes. The Raman intensities have been broadened by 25 cm^{-1}. The previous Raman active frequencies define a complex distribution which, in contrast to the simulated infrared spectra shown in Fig. 10, is more sensitive to the size and local atomic environment of our model BN cages. Even if in both Figs. 12(a) and 12(b) we observe, in agreement with experiments, the existence of intense bands located in the 200—600 cm^{-1} frequency range, we appreciate also notable contributions around 800 cm^{-1} which are completely absent in the measured data. However, it is important to remark from Fig. 12(c) that when the $B_{12}N_{12}@B_{48}N_{48}$ onion-like configuration is considered the Raman activity around 800 cm^{-1} is almost completely quenched. Notice also that, in contrast to the simulated infrared data, the distribution shown

in Fig. 12(c) is not defined by a simple superposition of the Raman spectra of the hollow cages. Here, the $B_{12}N_{12}@B_{48}N_{48}$ structure is characterized by the existence of an intense absorption band in the 200—600 cm^{-1} region having a double peak structure which, as already stated, is completely absent in the spectra of BN nanotubes, previously synthesized BN nanoparticles, as well as in all bulk boron-nitride polymorphs. The previous absorption bands are dominated by a complex mixture of tangential, stretching, as well as radial breathing modes and its location and structure is in acceptable agreement with the here-reported experimental Raman spectroscopy data shown in Fig. 9. The simulated Raman spectra of a model $B_{12}N_{12}@B_{48}N_{48}$–$B_{12}N_{12}@B_{48}N_{48}$ dimer is presented in Fig. 13. Notice that a similar distribution of Raman active frequencies is found, a result that clearly underlines the crucial role played by the individual boron-nitride nanoparticle units on the average properties observed on a macroscopic scale.

Finally, and following our XPS data, we consider the inclusion of oxygen species (defined by red circles) in our model $B_{12}N_{12}@B_{48}N_{48}$ onion-like configurations. We assume up to three O atoms chemisorbed on the external surface as well as between the layers in the $B_{12}N_{12}@B_{48}N_{48}$ structure. In Fig. 14 we show our optimized atomic configurations (as insets) and the simulated infrared spectra for the $B_{12}N_{12}@B_{48}N_{48}O_3$ [Fig. 14(a)] and $B_{12}N_{12}O_3@B_{48}N_{48}$ [Fig. 14(b)] particles. In both cases, the vibrational analysis reveals the existence of only positive frequencies, implying the formation of stable atomic configurations. From our calculations we obtain that oxygen atoms prefer to be attached to the external surface [Fig. 14(a)], having an energy difference of 3 eV when compared to the structure presented in Fig. 14(b). In the oxidized particles the HOMO—LUMO energy gap is further reduced being now equal to 2.8 and 2.5 eV in Figs. 14(a) and 14(b) respectively.

Notice that, in both figures, the B—N bond below the oxygen atoms is always broken yielding interatomic distances which vary from 2.1—2.3 Å. In addition, we found B—O and N—O bond lengths of the order of 1.45 Å. It is important to comment that, the previous interatomic separations have been observed in our HRTEM images a fact that corroborates further the existence of oxygen impurities within the samples. Finally, the calculated Raman spectra (not shown) of both $B_{12}N_{12}@B_{48}N_{48}O_3$ and $B_{12}N_{12}O_3@B_{48}N_{48}$ fullerenes remains practically unperturbed when compared to the one shown in Fig. 12(c).

4. Conclusions

In this work we have analyzed the formation, atomic structure, and electronic properties of various types of boron nitride (BN) nanostructures synthesized by using the mechanical milling methodology. Our synthetic protocol leads to the spontaneous formation of BN particles with diameters as small as ~7 nm which self-assemble into different porous hierarchical nanostructured materials such as two-dimensional layered structures, spheroidal configurations, and one-dimensional solid BN chains. Our chemical analysis reveals the existence of oxygen species in the surface of the samples, a fact that is in line with well know correlation between oxygen content and stability of the spherical morphology in BN nanoparticles. The vibrational spectroscopy measurements showed that both infrared and Raman spectra in combination with theoretical calculations can be used to obtain valuable information on the local atomic structure and general morphology of the samples. The B/N ratio of approximately 0.9, the porous nature of the hierarchical BN nanostructures, as well as the large HOMO—LUMO energy gap of 3 eV points to the

existence of highly stable BN nanomaterials with an enormous potential for gas storage applications, catalyst support, and gas adsorbent structures.

Acknowledgements

The authors would like to acknowledge the financial support from CONACyT through grants 169345, 164594, and 297004. Computer resources from the Acarus Supercomputer Center of the Universidad de Sonora, Sonora, México, as well as from the National Supercomputer Center (NSC) of IPICyT, México are also acknowledged.

5. References

1. Lei, W.; Portehault, D.; Liu, D.; Qin, S.; Chen, Y., Porous Boron Nitride Nanosheets for Effective Water Cleaning. *Nat Commun* **2013**, *4*, 1777.
2. Deepika; Li, L. H.; Glushenkov, A. M.; Hait, S. K.; Hodgson, P.; Chen, Y., High-Efficient Production of Boron Nitride Nanosheets Via an Optimized Ball Milling Process for Lubrication in Oil. *Sci. Rep.* **2014**, *4*.
3. Pouch, J. J.; Alterovitz, S. A., A Review Of: "Synthesis and Properties of Boron Nitride". *Materials and Manufacturing Processes* **1991**, *6*, 373-374.
4. Liu, D.; Lei, W.; Qin, S.; Chen, Y., Template-Free Synthesis of Functional 3d Bn Architecture for Removal of Dyes from Water. *Sci. Rep.* **2014**, *4*.
5. Zhi, C.; Bando, Y.; Tang, C.; Kuwahara, H.; Golberg, D., Large-Scale Fabrication of Boron Nitride Nanosheets and Their Utilization in Polymeric Composites with Improved Thermal and Mechanical Properties. *Advanced Materials* **2009**, *21*, 2889-2893.
6. Liu, Z., et al., Ultrathin High-Temperature Oxidation-Resistant Coatings of Hexagonal Boron Nitride. *Nat Commun* **2013**, *4*.
7. Eichler, J.; Lesniak, C., Boron Nitride (Bn) and Bn Composites for High-Temperature Applications. *Journal of the European Ceramic Society* **2008**, *28*, 1105-1109.
8. Lee, K. H.; Shin, H.-J.; Lee, J.; Lee, I.-y.; Kim, G.-H.; Choi, J.-Y.; Kim, S.-W., Large-Scale Synthesis of High-Quality Hexagonal Boron Nitride Nanosheets for Large-Area Graphene Electronics. *Nano Letters* **2012**, *12*, 714-718.
9. Rubio, A.; Corkill, J. L.; Cohen, M. L., Theory of Graphitic Boron Nitride Nanotubes. *Physical Review B* **1994**, *49*, 5081-5084.
10. Chopra, N. G.; Luyken, R. J.; Cherrey, K.; Crespi, V. H.; Cohen, M. L.; Louie, S. G.; Zettl, A., Boron Nitride Nanotubes. *Science* **1995**, *269*, 966-967.
11. Blase, X.; Rubio, A.; Louie S. G. and Cohen, M. L. , Stability and Band Gap Constancy of Boron Nitride Nanotubes. *Europhys. Lett* **1994** *28*, 335.
12. Gao, R.; Yin, L.; Wang, C.; Qi, Y.; Lun, N.; Zhang, L.; Liu, Y.-X.; Kang, L.; Wang, X., High-Yield Synthesis of Boron Nitride Nanosheets with Strong Ultraviolet

Cathodoluminescence Emission. *The Journal of Physical Chemistry C* **2009**, *113*, 15160-15165.
13. Lourie, O. R.; Jones, C. R.; Bartlett, B. M.; Gibbons, P. C.; Ruoff, R. S.; Buhro, W. E., Cvd Growth of Boron Nitride Nanotubes. *Chemistry of Materials* **2000**, *12*, 1808-1810.
14. Tang, C.; Bando, Y.; Huang, Y.; Zhi, C.; Golberg, D., Synthetic Routes and Formation Mechanisms of Spherical Boron Nitride Nanoparticles. *Advanced Functional Materials* **2008**, *18*, 3653-3661.
15. Salles, V.; Bernard, S.; Li, J.; Brioude, A.; Chehaidi, S.; Foucaud, S.; Miele, P., Design of Highly Dense Boron Nitride by the Combination of Spray-Pyrolysis of Borazine and Additive-Free Sintering of Derived Ultrafine Powders. *Chemistry of Materials* **2009**, *21*, 2920-2929.
16. Bernard, S.; Salles, V.; Li, J.; Brioude, A.; Bechelany, M.; Demirci, U. B.; Miele, P., High-Yield Synthesis of Hollow Boron Nitride Nano-Polyhedrons. *Journal of Materials Chemistry* **2011**, *21*, 8694-8699.
17. Koi, N.; Oku, T.; Narita, I.; Suganuma, K., Synthesis of Huge Boron Nitride Cages. *Diamond and Related Materials* **2005**, *14*, 1190-1192.
18. Golberg, D.; Bando, Y.; Stéphan, O.; Kurashima, K., Octahedral Boron Nitride Fullerenes Formed by Electron Beam Irradiation. *Applied Physics Letters* **1998**, *73*, 2441-2443.
19. Stéphan, O.; Bando, Y.; Loiseau, A.; Willaime, F.; Shramchenko, N.; Tamiya, T.; Sato, T., Formation of Small Single-Layer and Nested Bn Cages under Electron Irradiation of Nanotubes and Bulk Material. *Applied Physics A* **1998**, *67*, 107-111.
20. Oku, T.; Hirano, T.; Kuno, M.; Kusunose, T.; Niihara, K.; Suganuma, K., Synthesis, Atomic Structures and Properties of Carbon and Boron Nitride Fullerene Materials. *Materials Science and Engineering: B* **2000**, *74*, 206-217.
21. Oku, T.; Kuno, M., Synthesis, Argon/Hydrogen Storage and Magnetic Properties of Boron Nitride Nanotubes and Nanocapsules. *Diamond and Related Materials* **2003**, *12*, 840-845.
22. Oku, T.; Kuno, M.; Narita, I., Hydrogen Storage in Boron Nitride Nanomaterials Studied by Tg/Dta and Cluster Calculation. *Journal of Physics and Chemistry of Solids* **2004**, *65*, 549-552.
23. Frisch, M. J., et al. *Gaussian 09*, Gaussian, Inc.: Wallingford, CT, USA, 2009.
24. Perdew, J. P.; Burke, K.; Ernzerhof, M., Perdew, Burke, and Ernzerhof Reply. *Physical Review Letters* **1998**, *80*, 891-891.
25. Binkley, J. S.; Pople, J. A.; Hehre, W. J., Self-Consistent Molecular Orbital Methods. Small Split-Valence Basis Sets for First-Row Elements. *Journal of the American Chemical Society* **1980**, *102*, 939.
26. Xia, Z. P.; Li, Z. Q., Structural Evolution of Hexagonal BN and Cubic BN During Ball Milling. *Journal of Alloys and Compounds* **2007**, *436*, 170-173.
27. Reich, S.; Ferrari, A. C.; Arenal, R.; Loiseau, A.; Bello, I.; Robertson, J., Resonant Raman Scattering in Cubic and Hexagonal Boron Nitride. *Physical Review B* **2005**, *71*, 205201.
28. Arenal, R.; Ferrari, A. C.; Reich, S.; Wirtz, L.; Mevellec, J. Y.; Lefrant, S.; Rubio, A.; Loiseau, A., Raman Spectroscopy of Single-Wall Boron Nitride Nanotubes. *Nano Letters* **2006**, *6*, 1812-1816.

29. Oku, T.; Narita, I.; Nishiwaki, A., Formation and Structures of $B_{36}N_{36}$ and $Y@B_{36}N_{36}$ Clusters Studied by High-Resolution Electron Microscopy and Mass Spectrometry. *Journal of Physics and Chemistry of Solids* **2004**, *65*, 369-372.
30. Oku, T.; Nishiwaki, A.; Narita, I., Formation and Atomic Structure of B12n12 Nanocage Clusters Studied by Mass Spectrometry and Cluster Calculation. *Science and Technology of Advanced Materials* **2004**, *5*, 635-638.
31. Enyashin, A. N.; Makurin, Y. N.; Ivanovskii, A. L., Structure and Electronic Characteristics of New Graphyne-Like Fullerenes of Boron Nitride: Quantum-Chemical Modelling. *Theoretical and Experimental Chemistry* **2004**, *40*, 71-76.
32. Oku, T.; Narita, I.; Nishiwaki, A., Synthesis, Atomic Structures, and Electronic States of Boron Nitride Nanocage Clusters and Nanotubes. *Materials and Manufacturing Processes* **2004**, *19*, 1215-1239.

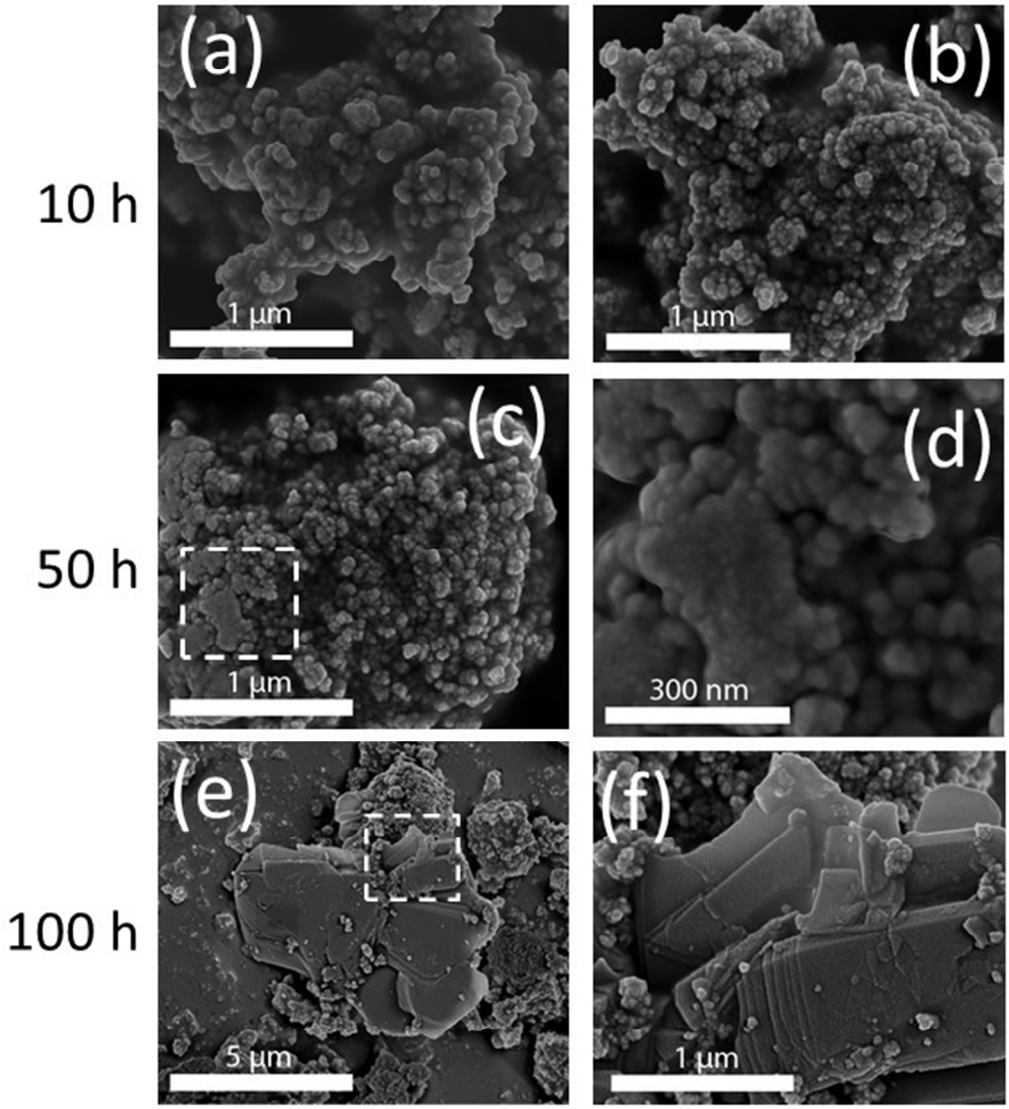

Figure 1. SEM images of the as-prepared BN nanostructures synthesized at different milling hours using the traditional ball milling methodology.

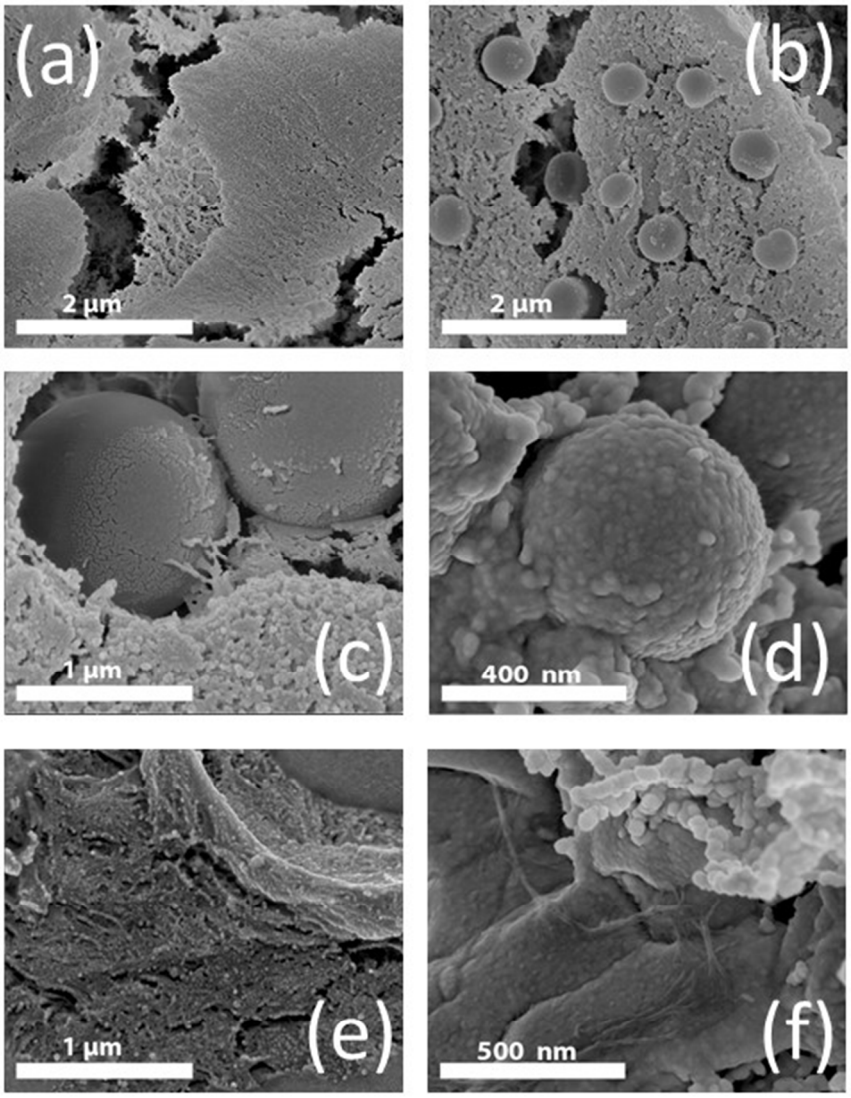

Figure 2. SEM images of BN nanostructures synthesized after 100 h of milling and heated at 1000 °C for 16 h.

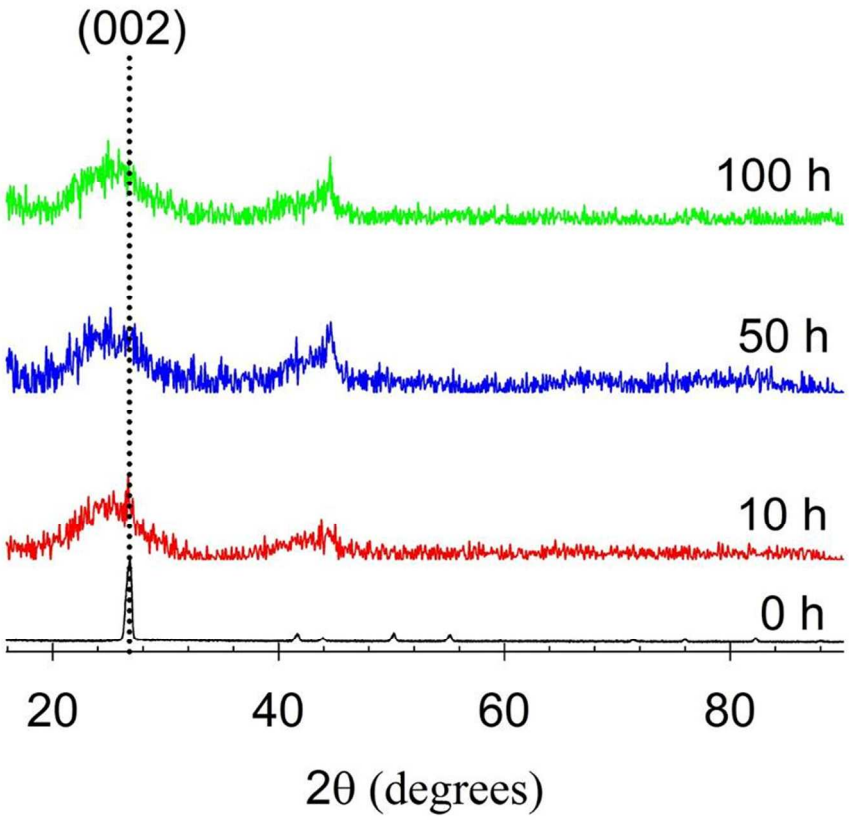

Figure 3. Powder XRD patterns of the BN products prepared at different milling hours.

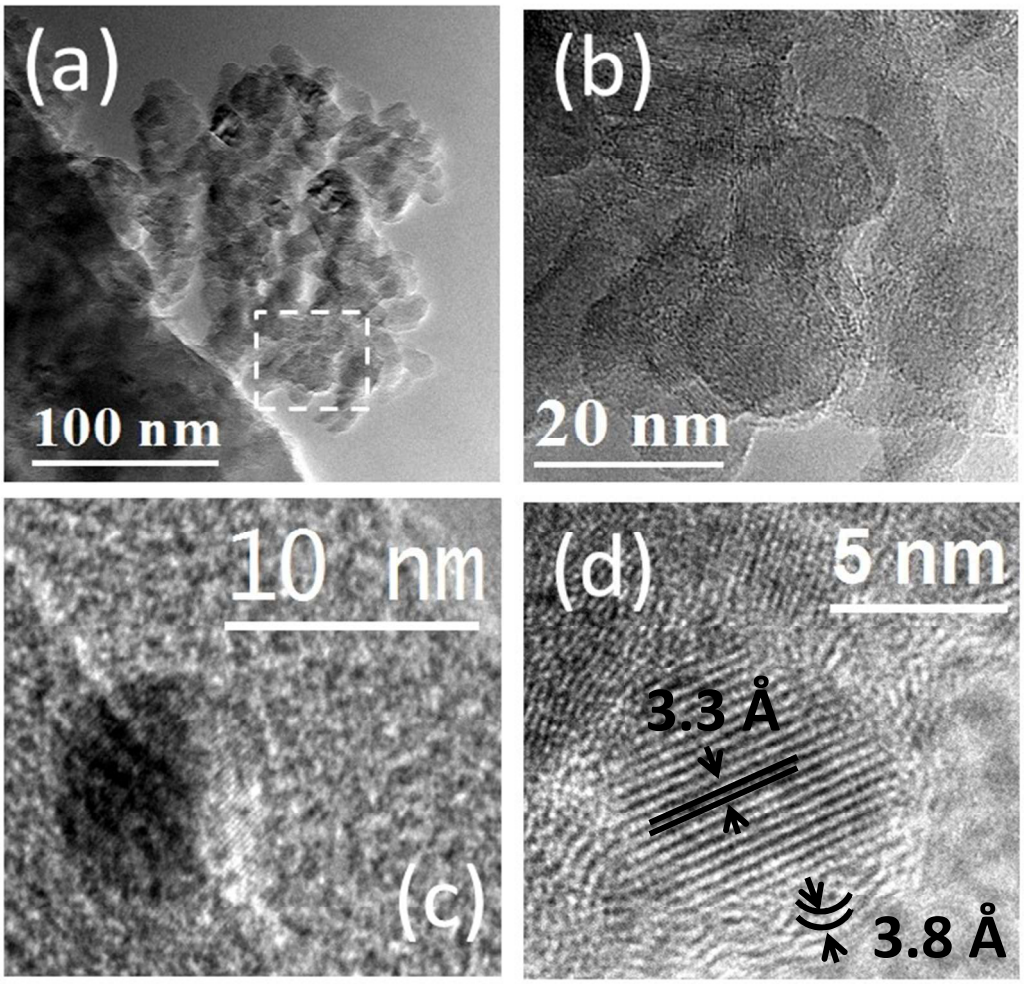

Figure 4. HRTEM images of BN nanostructures synthesized after 100 h of milling and heated at 1000 °C for 16 h.

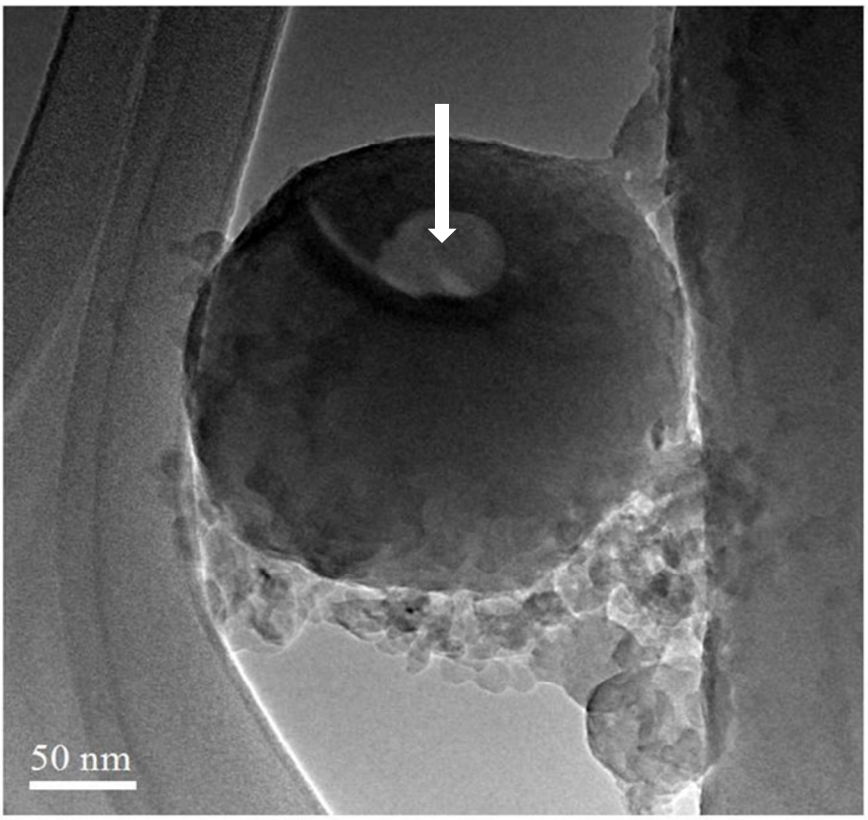

Figure 5. HRTEM image of an isolated BN hierarchical nanosphere of ~300 nm in diameter which was subjected to an incident electron beam of 300 KeV for 2 min.

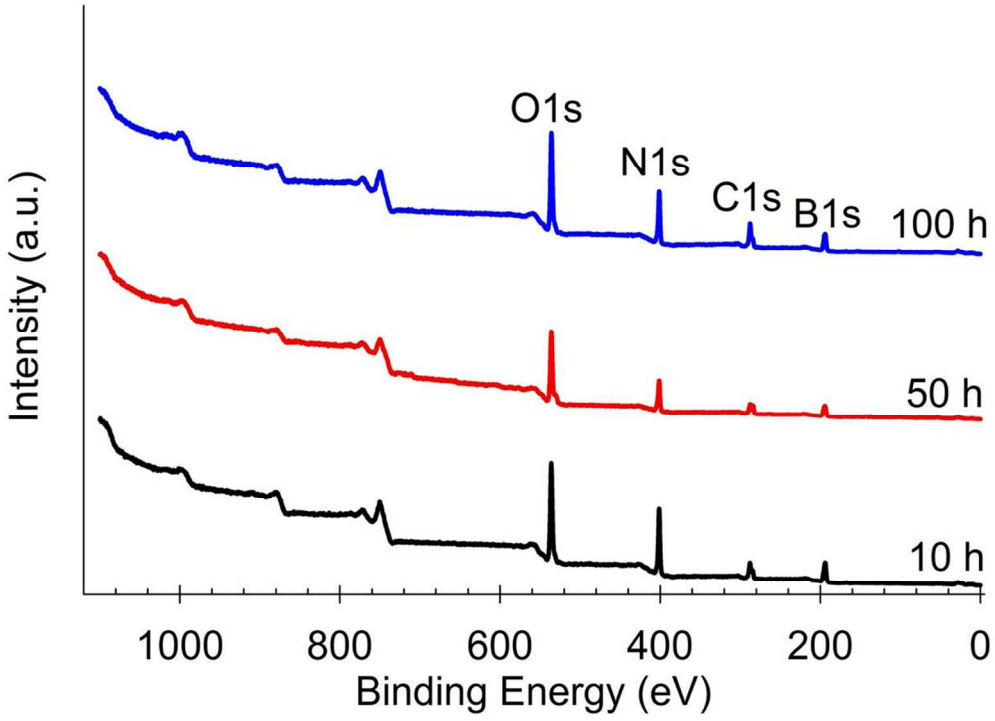

Figure 6. XPS spectra of the BN products prepared at different milling hours.

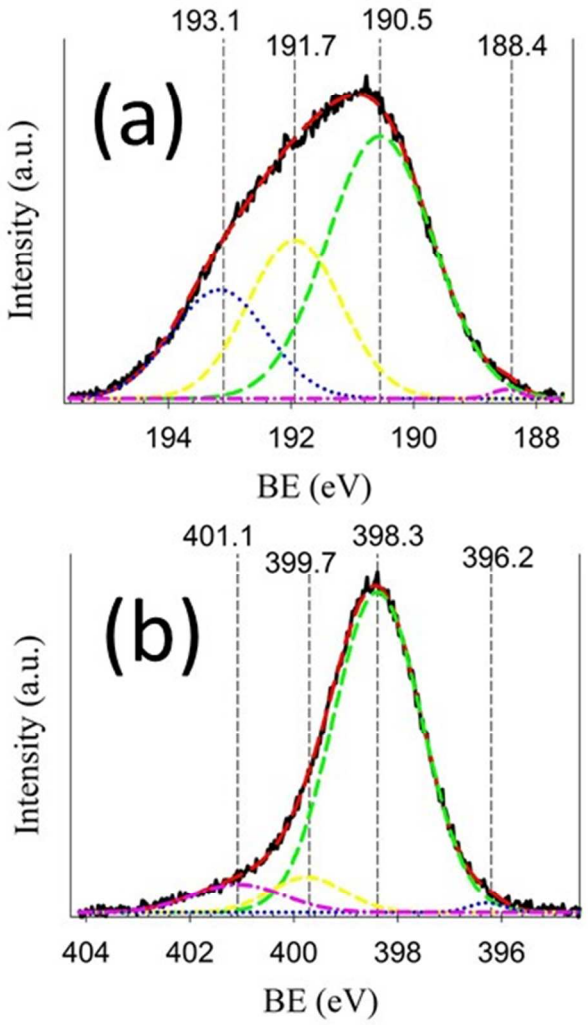

Figure 7. Deconvolution with symmetrical Gaussian-Lorentzian curve fitting of the (a) B 1s and (b) N 1s XPS spectra for a BN sample synthesized after 100 h of milling and heated at 1000 °C for 16 h.

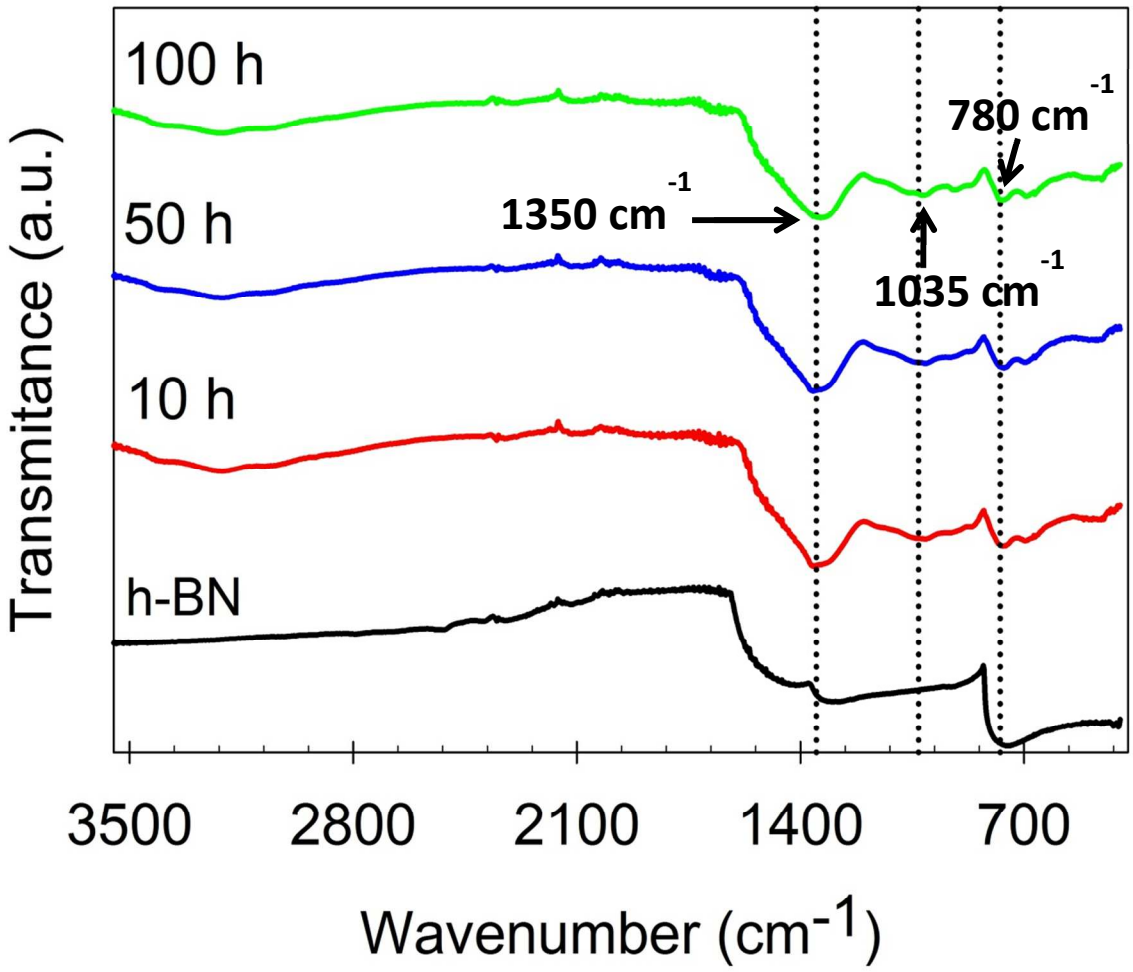

Figure 8. FTIR spectra of the BN products prepared at different milling hours.

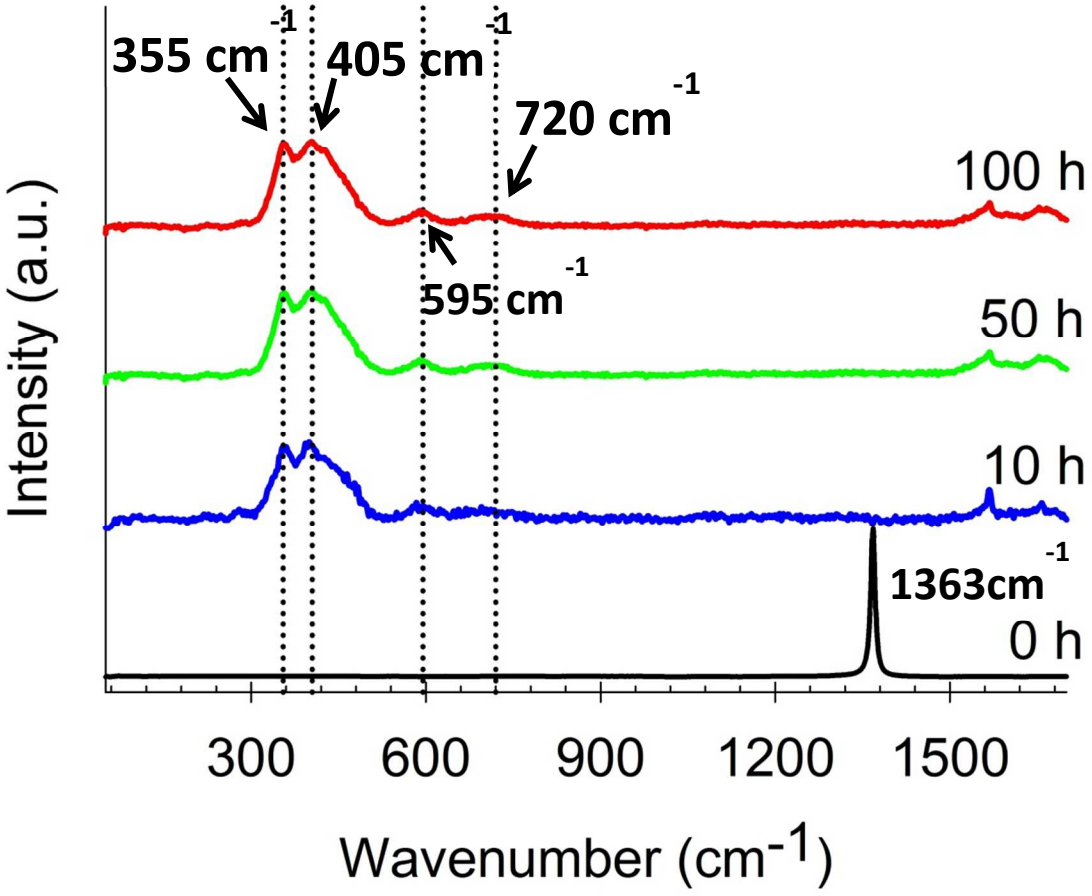

Figure 9. Raman spectra of the BN products prepared at different milling hours. We include the Raman spectra of bulk *h*-BN (black line) for comparison.

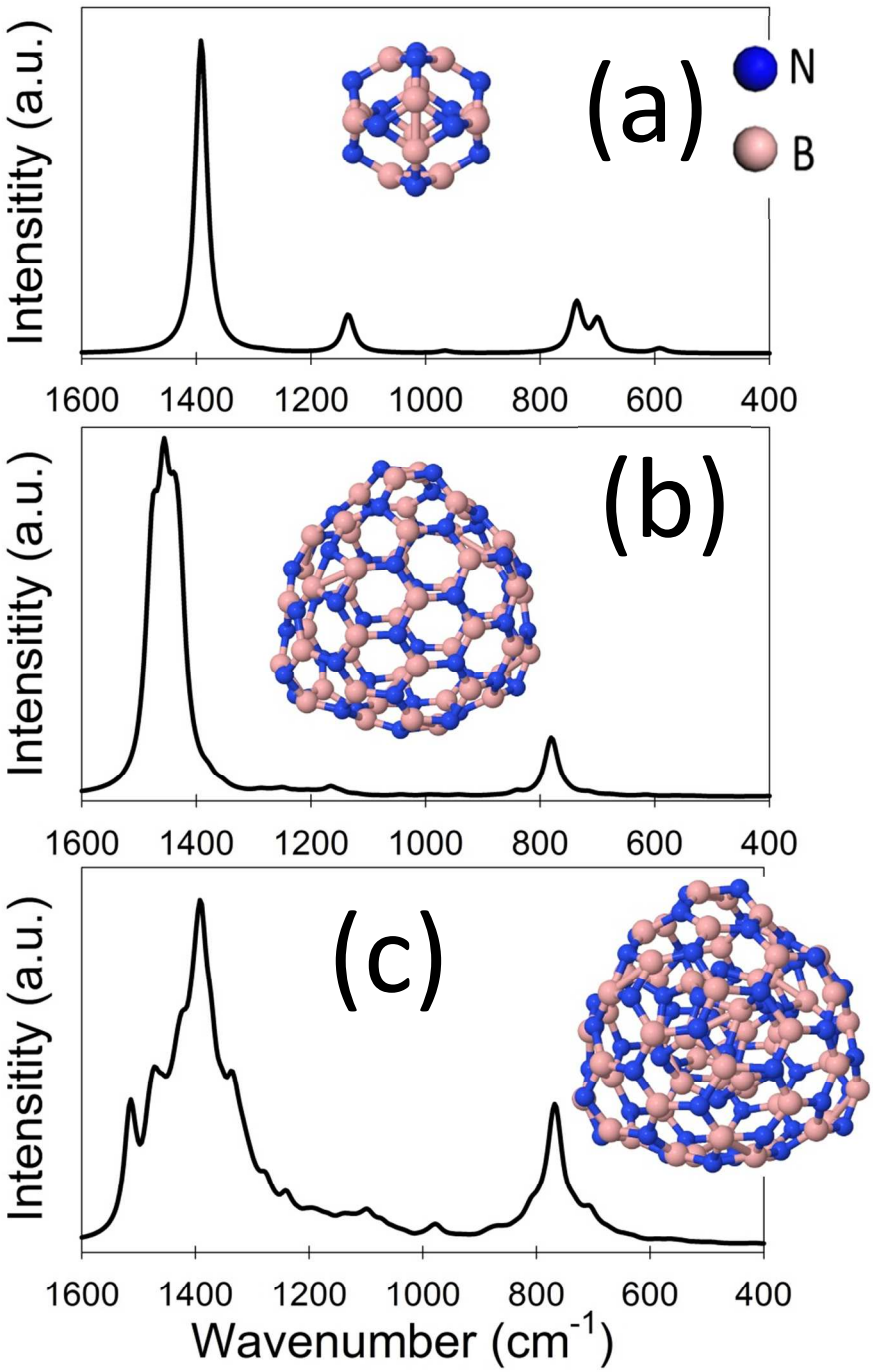

Figure 10. Simulated infrared spectra of our model (a) $B_{12}N_{12}$, (b) $B_{48}N_{48}$, and (c) $B_{12}N_{12}@B_{48}N_{48}$ particles.

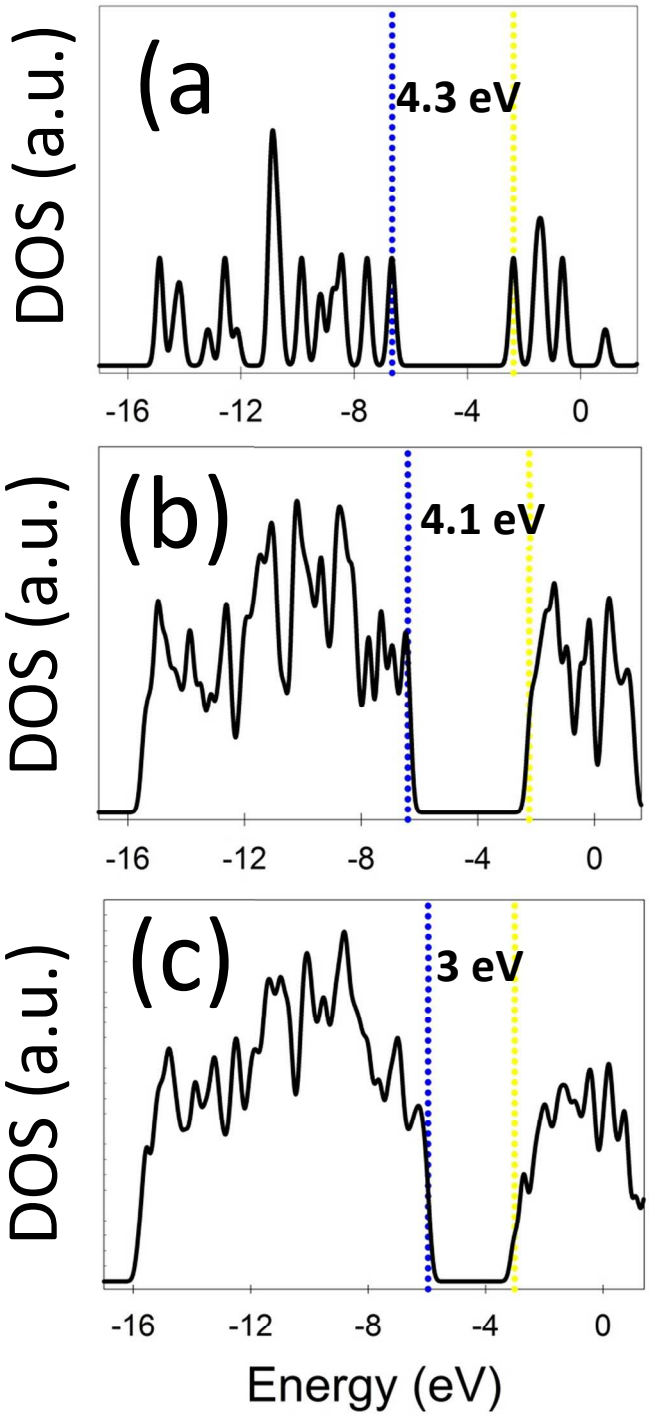

Figure 11. Calculated DOS for our model (a) $B_{12}N_{12}$, (b) $B_{48}N_{48}$, and (c) $B_{12}N_{12}@B_{48}N_{48}$ particles.

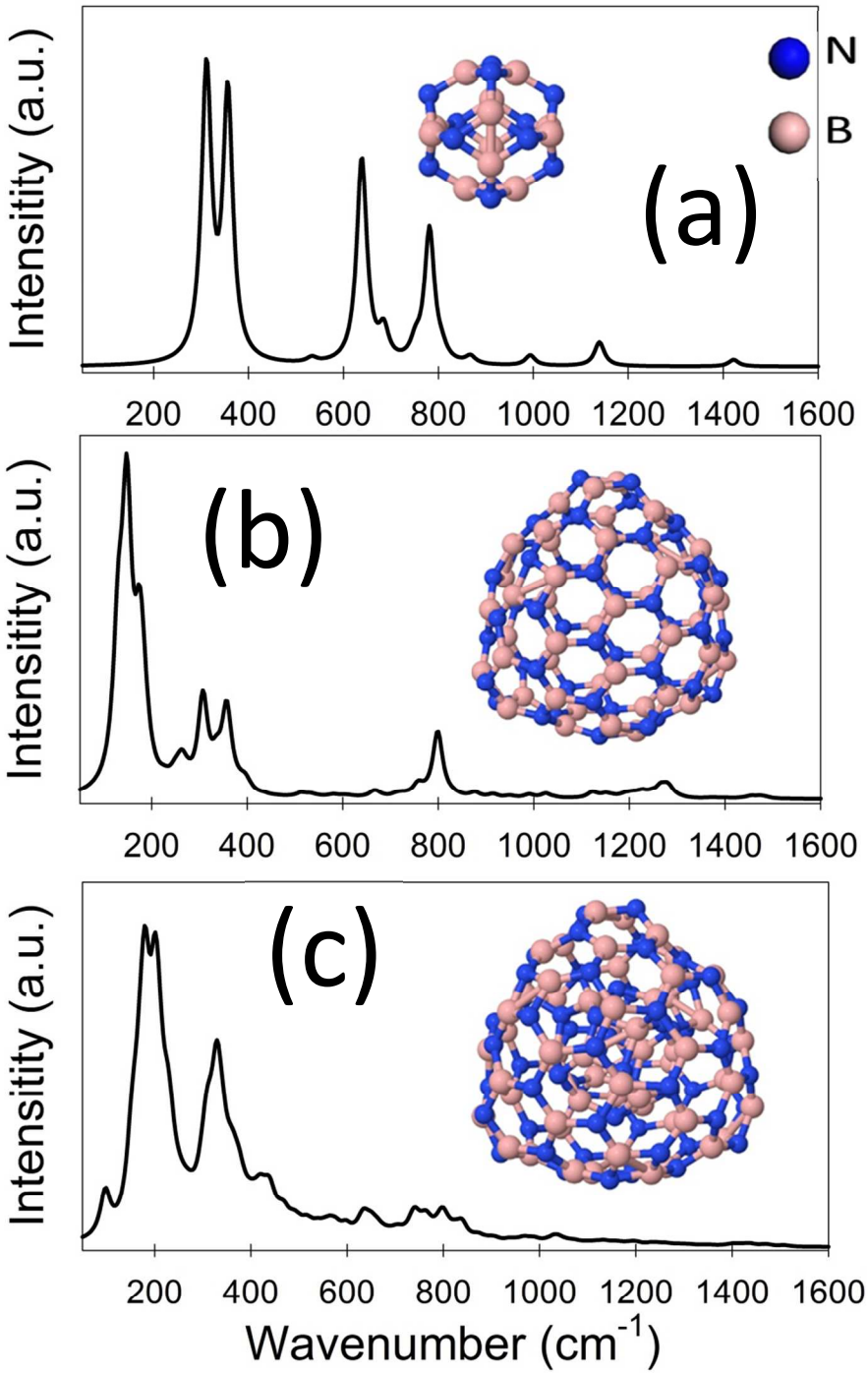

Figure 12. Simulated Raman spectra of our model (a) $B_{12}N_{12}$, (b) $B_{48}N_{48}$, and (c) $B_{12}N_{12}@B_{48}N_{48}$ particles.

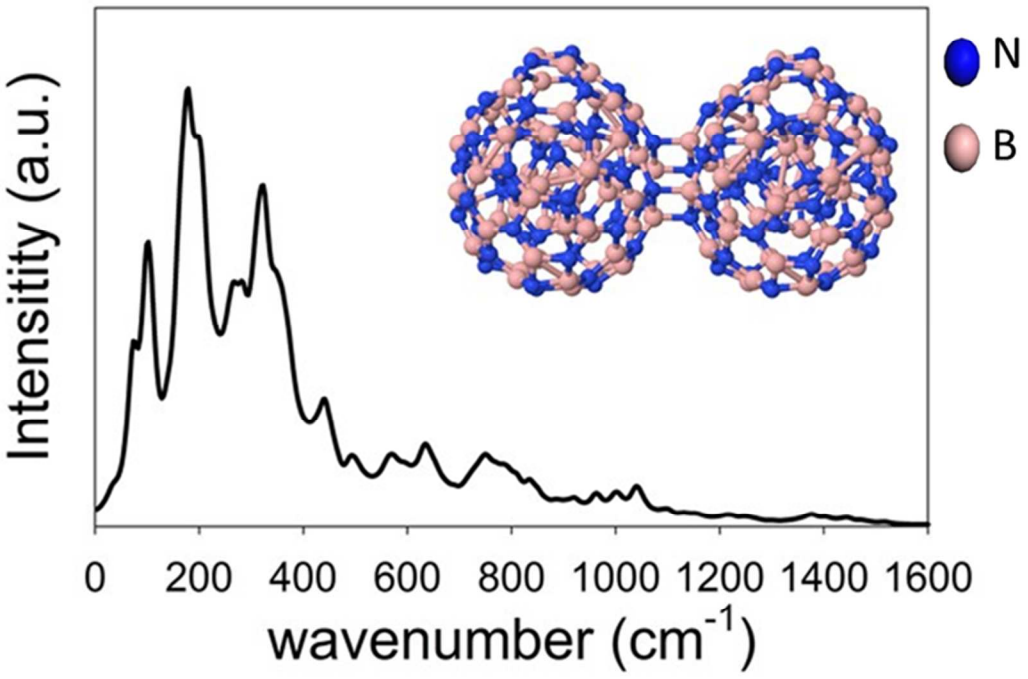

Figure 13. Simulated Raman spectra of a model $B_{12}N_{12}@B_{48}N_{48}$–$B_{12}N_{12}@B_{48}N_{48}$ dimer.

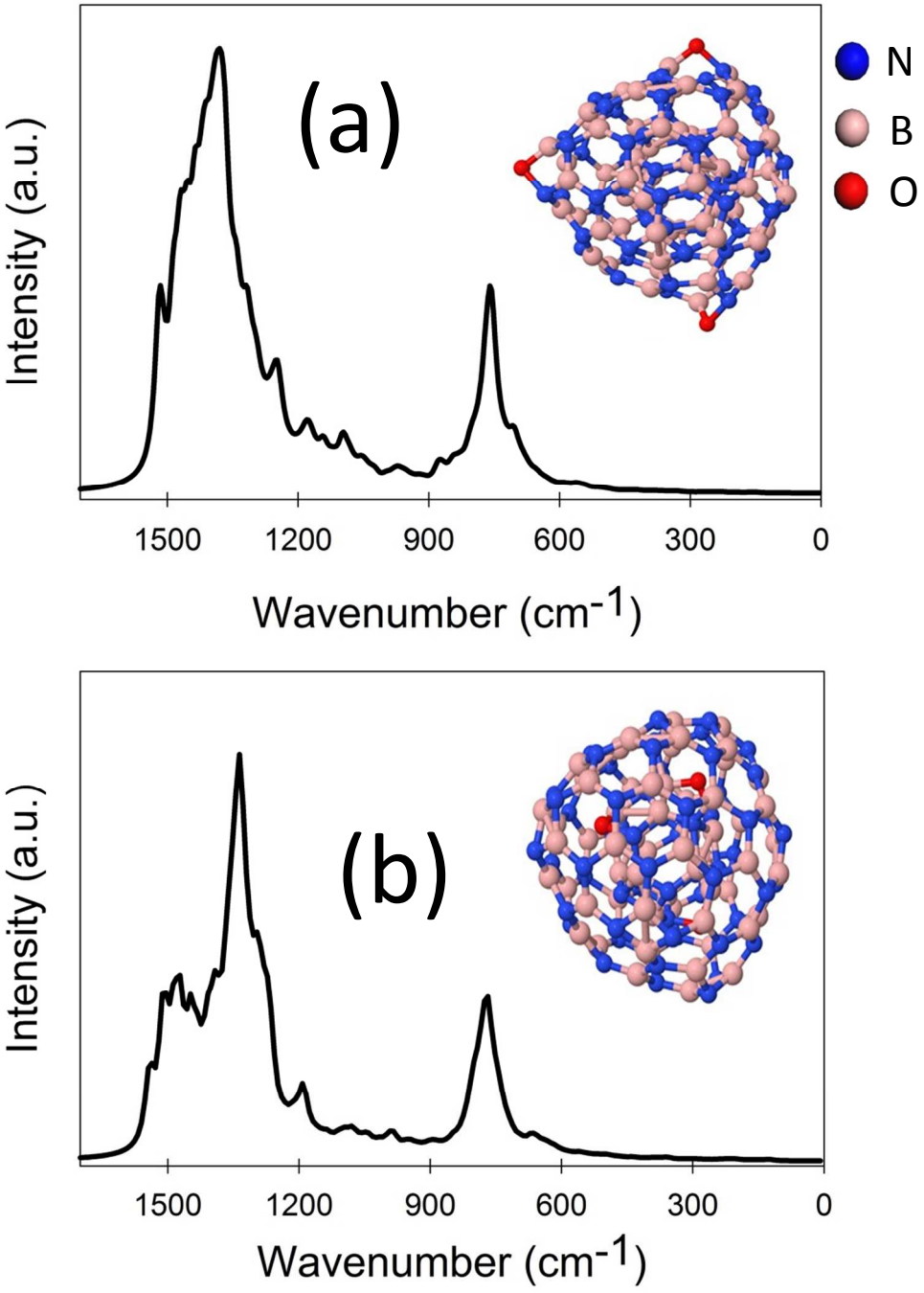

Figure 14. Simulated infrared spectra of our model oxygen-containing (a) $B_{12}N_{12}@B_{48}N_{48}O_3$ and (b) $B_{12}N_{12}O_3@B_{48}N_{48}$ particles.

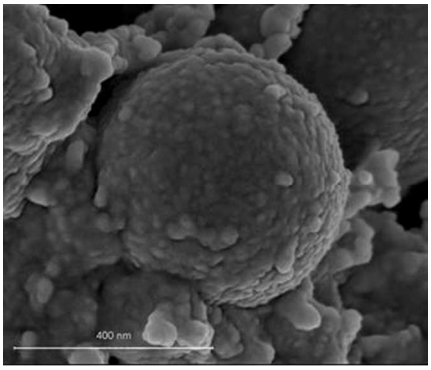

TOC image